Energy xxx (2016) 1–11

Contents lists available at ScienceDirect

Energy

journal homepage: www.elsevier.com/locate/energy

Exploring the potential for waste heat recovery during metal casting with thermoelectric generators: On-site experiments and mathematical modeling

Marit Takla Børset [a], Øivind Wilhelmsen [b, c], Signe Kjelstrup [a], Odne Stokke Burheim [c, *]

[a] Department of Chemistry, Norwegian University of Science and Technology, NO-7491 Trondheim, Norway
[b] SINTEF Energy Research, N-7465 Trondheim, Norway
[c] Dep. Electr. Engin. Renewable Energy, Faculty of Technology, NTNU, Trondheim, Norway

ARTICLE INFO

Article history:
Received 27 April 2016
Received in revised form
9 September 2016
Accepted 26 October 2016
Available online xxx

Keywords:
Seebeck effect
Thermoelectric generator (TEG)
Radiative heat source
Transient heat source
Industrial experiments
Mathematical model

ABSTRACT

Thermoelectric power generators are scalable and simple systems for recovering waste-heat disposed by the industry. We combine on-site measurements and a mathematical model to study the potential for power generation with this technology from heat available from casting of silicon. We implement a 0.25 m^2 thermoelectric generator (TEG), based on bismuth-tellurium modules, in the casting area of a silicon plant. The measured peak power is 160 W m^{-2} and the corresponding maximum temperature difference across the modules is 100 K. We predict a large potential to increase the power generated beyond the measured values. For a two-fold increase of the heat transfer coefficient at the cold side, and by moving the generator closer to the heat source, we predict that the power output can reach 900 W m^{-2}. By tailoring the design of the TEG to the conditions encountered in the industrial facility, it is possible to generate more power with less thermoelectric material. We provide guidelines on how to design thermoelectric systems to maximize the power generation from waste heat given off from silicon during casting.

1. Introduction

Access to energy in the right form, at the right time, and at the right place is a premise for our society to continue to prosper. Accordingly, with the stipulated population growth and increase in welfare, the power production must continue to grow, however in appropriate ways [1]. The power supply for a modern society must deal with production, storage and distribution and must come from diverse sources. Moreover, for the society to be sustainable the sources of energy supply must eventually be renewable. Reusing a waste, such as waste heat, is considered a conditional renewable energy source. Furthermore, meeting the future need of power supply requires that we also deal with the concept of energy quality. Electric energy is for instance of greater value than thermal energy. Heat at high temperatures is of greater value than at lower temperatures. Heat on demand is of greater value than intermittent and distributed heat. Thermoelectric generators represent a scalable and robust technology to convert waste-heat to high quality electricity. In this paper, we investigate the implementation of thermoelectric generators in the metal casting industry, where intermittent high quality heat is available alongside with a power demand.

Thermoelectric generators (TEGs) convert a thermal potential (temperature difference) directly to an electric potential (voltage) when heat passes through the generators [2]. To our knowledge, this effect was first discovered in the 19th century by Seebeck [3]. The Seebeck effect occurs when two different charge conductors (*e.g.*, p- and n-type semiconductors) are coupled in series via two connections (A-B-A) and when the connections are at different temperatures (A-B at T_1 and B-A at T_2). As long as the temperatures T_1 and T_2 deviate, we can measure an electric potential in the circuit that is proportional to the temperature difference, where the slope equals the Seebeck coefficient, α, of the pair of conductors. Thermoelectric generators are scalable systems, ranging from micro-watts to kilo-watts applications [4,5]. The efficiency of a TEG relative to the Carnot efficiency is typically below 5%, which is

* Corresponding author.
E-mail addresses: marit.takla@gmail.com (M.T. Børset), oivind.wilhelmsen@sintef.no (Ø. Wilhelmsen), signe.kjelstrup@ntnu.no (S. Kjelstrup), odne.s.burheim@ntnu.no (O.S. Burheim).

http://dx.doi.org/10.1016/j.energy.2016.10.109

significantly lower than the same relative efficiency of competing technologies such as steam turbine systems and organic Rankine cycle systems, where steam turbine systems can have efficiencies relative to the Carnot efficiency that exceed 40% [6]. The main advantages of TEGs compared to alternative technologies are their size (plates of a few millimeters), scalability, fairly simple constructions (no moving parts), weight (used for mobile applications) and flexibility (fitting to intermittent heat sources) [6].

There are many materials available for use when it comes to thermoelectric generators. Those most commonly referred to are inorganic, and are applicable for temperatures up to 550 K (BiSnTe-based, BiSbTe-based), up to 800 K (PbTeSe, PbSe-based) or up to 1200 K (SiGe) [6]. One obvious goal in the development of thermoelectric generators is to have a large Seebeck coefficient (α) for the materials. This is observed for conducting organic systems [7,8] as well as for membrane and super-capacitor systems [9–11]. Recently, Børset et al. [12] and Kang et al. [13] reported very high Seebeck coefficients (0.9 mV/K $< \alpha <$ 1.3 mV/K) using molten carbonate cells reversible to carbon dioxide and oxygen for the temperature range above 650 K.

However, to develop TEGs requires more than just high Seebeck coefficients [6,14,15]. Cost, energetically and financial, obviously have to be taken into account. On the energetic side, the figure of merit *ZT* is frequently used to characterize the capability of a material to convert heat to electricity [6] and should be as large as possible to obtain a high conversion efficiency. The parameter includes the material's Seebeck coefficient, electrical conductivity and the thermal conductivity (measured at zero electrical current). Fiscal costs are related to raw material costs, purification and assembly of the TEG module in addition to the auxiliary system (cooling and heating system) [14,15]. Regardless of the source, it will always be beneficial for the TEG cost to reduce the module fill-factor (f_{Am}), *i.e.* the fraction of the cross section in a thermoelectric module that is filled with active material, and the conductor thickness [14,15]. There is, however, a complex interplay between thermal and electrical properties, both dependent on cross-sectional areas and thicknesses of the conductors, and the optimum design is a trade-off of these properties [15]. Higher temperature difference is beneficial to power generation, and can be obtained by reducing the cross-sectional areas of the conductors and by increasing the thicknesses. At a given conductor thickness, the thermal conductivity of the thermoelectric module can be reduced by reducing the fill-factor, but lowering the filling degree too much will make the temperature differences across the TEG module increase to an extent that the materials cannot sustain and thus lowering the feet length is required. This means that if correctly optimized, one can have more power with less use of material. This is an attractive possibility we shall further explore in this work.

Regardless of the TEG module end cost, one must always make sure to operate the TEG within the feasible temperature range for material stability. Many materials have been tested and evaluated with respect to performance from a *ZT*-factor, module feet length, and filling degree parametric point of view [14,15], but very few studies look into actual implementation outside the laboratory [15,16]. Several works have studied thermoelectric generators from a purely theoretical perspective [17–25], through a combination of theory and laboratory experiments [26–29] or through laboratory experiments [30–32]. However, to be able to enhance the performance of TEGs for industrial waste heat recovery, it is essential to combine on-site experiments with mathematical modeling.

In this work, we shall take the next step towards industrial applications of TEGs by combining on-site experiments and mathematical modeling to investigate the potential of this technology for power generation from heat available during casting of silicon. Previous work has documented that by recovering the waste heat during silicon casting, it is possible to increase the exergetic efficiency from 0.33 to 0.41, i.e. by 24% [33,34]. In silicon production, silicon is cast in batches where heat is sporadically available. A TEG could thus provide the power needed during the casting process. We develop in this work a mathematical model that has a sufficient level of complexity to capture the main characteristics of the experimental results, but is flexible enough to explore a large range of possible TEG configurations. By taking advantage of the model and the measurements, we show how to enhance the power output of the TEG with less use of material. Moreover, we propose a novel methodology for designing TEG generator systems, opposed to evaluation of single modules which is what is more common in the literature.

The outline of the paper is as follows: In Sec. 2 we give the details of the thermoelectric generator, the casting situation and the testing facilities. The experimental set-up establishes a base case for the model. We then describe the mathematical model, the model parameters applicable to the experimental set-up and give the calculation details in Sec. 3. In Sec. 4 we discuss first the experimental results and compare the model predictions to the measured data to verify that the model captures the experimental results. We then use the model to study how changes in design and location affect the power output and reveal a significant potential to tailor the design of thermoelectric generators to recover more waste heat from silicon casting and simultaneously use less material.

2. Experimental

In this section we give the details of the thermoelectric generator [16], the casting process, testing facilities and testing procedure.

2.1. System description

A thermoelectric generator was constructed consisting of 36 thermoelectric modules based on bismuth tellurium (TEP-1264-1.5, Thermonamic, China). The TEP-1264-1.5 module consisted of 126 pairs of p- and n-type semiconductors connected electrically in series and kept between two ceramic plates (electrically non-conductive material in Fig. 3). Each module was square-shaped of size 40 mm × 40 mm. Thus, for 36 thermoelectric modules the total module surface area was 0.0576 m^2. The modules were arranged in a six by six matrix, connected electrically in series of six ($N_s = 6$), and six series were connected in parallel ($N_p = 6$), see Fig. 1.

In addition to the thermoelectric modules, the generator consisted of a heating block and a cooling block; the modules were sandwiched between them. The heating block and the cooling block were made of aluminum because aluminum has high thermal conductivity, good machinability and it is easily accessible. Soft graphite sheets with a very high thermal conductivity were used as thermal interface material between the thermoelectric modules and the aluminum plates to ensure a low thermal resistance. The heating block was made of 36 square-shaped units (10 mm thick), one for each thermoelectric module. Each unit's surface was 80 mm × 80 mm on the side facing the heat source, while the surface was 49 mm × 49 mm for the side in contact with the thermoelectric module. The purpose of this design (see Fig. 2a) was to concentrate the heat flux into the thermoelectric modules. The cooling block was made of a 25 mm thick aluminum plate (0.5 m × 0.5 m) where water was circulating in a copper pipe (10 mm in diameter and 3.2 m long). The copper pipe was fixed in a channel which was machined into the aluminum plate. We used tap water for cooling (6.0 ± 0.5) °C and measured the inlet and the

Please cite this article in press as: Børset MT, et al., Exploring the potential for waste heat recovery during metal casting with thermoelectric generators: On-site experiments and mathematical modeling, Energy (2016), http://dx.doi.org/10.1016/j.energy.2016.10.109

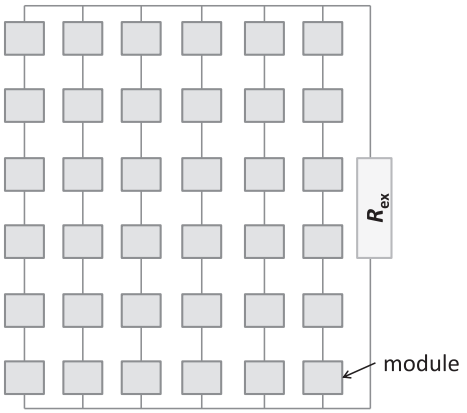

Fig. 1. The thermoelectric generator consisted of an array of 36 thermoelectric modules, connected electrically in series of six (N_s) and six series connected in parallel (N_p). The thermoelectric system is connected to an external circuit with and external load R_{ex}.

generator (left) and a cut through the generator (right). The cut-through shows one thermoelectric module (TM) kept between one heating block unit (HB) and a part of the cooling block (CB). We used K-type thermocouples to measure the heating block and the cooling block temperatures, T_{hb} and T_{cb}, respectively, see Figs. 2a and 3. The thermocouples were inserted into holes (1 mm in diameter). Five thermocouples were included in the heating block, indicated by numbers 1–5 in Fig. 2a. Four thermocouples were included in the cooling block, indicated by numbers 1–4. The thermoelectric generator was heated by radiant heat. Because aluminum has a relatively low emissivity coefficient ($\varepsilon = 0.04–0.09$ for non-oxidized aluminum [35]), we painted the front side of the heating block black with high temperature paint.

2.2. The casting situation and testing facilities

At the plant, silicon was cast from a ladle containing 8000–9000 kg of silicon into molds placed next to each other on a

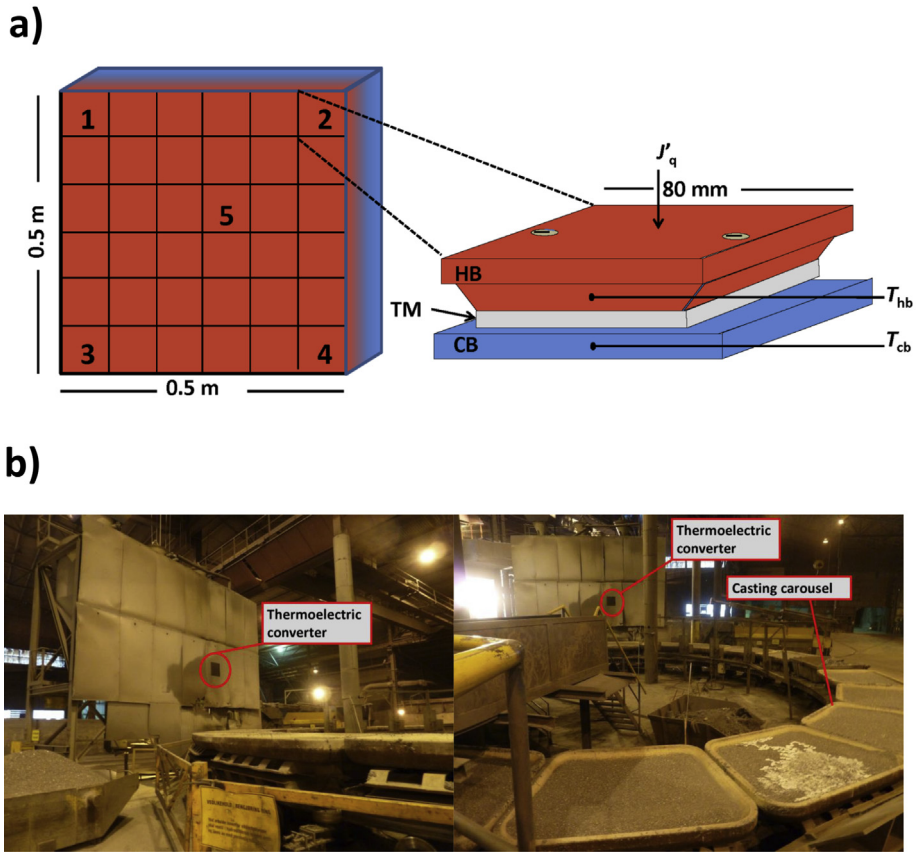

Fig. 2. A) The thermoelectric power generator and an extracted repeated unit, showing one thermoelectric module (TM) kept between the cooling block (CB) and the heating blocks (HB). The HBs are heated mainly by radiant heat (J'_q). The temperature is measured in the HB and the CB (T_{hb} and T_{cb}, see Fig. 3). The numbers 1–5 indicate thermocouple locations. B) The casting area at the silicon plant and the thermoelectric generator installed in the casting area.

outlet temperature with PT100 elements. The cooling block gave support to the thermoelectric generator construction. The thermoelectric modules were assembled between the heating block and the cooling block, using screws (4 mm in diameter) running through the heating block and the cooling block. The screws were not insulated and thus represent a possible heat leakage. We used two screws per heating block unit.

Fig. 2a shows a schematic drawing of the thermoelectric

rotating ring named the casting carousel. When one mold was filled with silicon, the carousel rotated so that silicon could be poured into the next mold until the ladle was emptied. To cast one ladle took 25–35 min and occurred roughly every other hour. In the ladle, the temperature of the silicon was initially 1450 °C. The melting point of silicon is close to 1410 °C. A benefit of using heat from the solidification process is that the heat is present near this temperature for very long time. That is, we seek high temperature

Please cite this article in press as: Børset MT, et al., Exploring the potential for waste heat recovery during metal casting with thermoelectric generators: On-site experiments and mathematical modeling, Energy (2016), http://dx.doi.org/10.1016/j.energy.2016.10.109

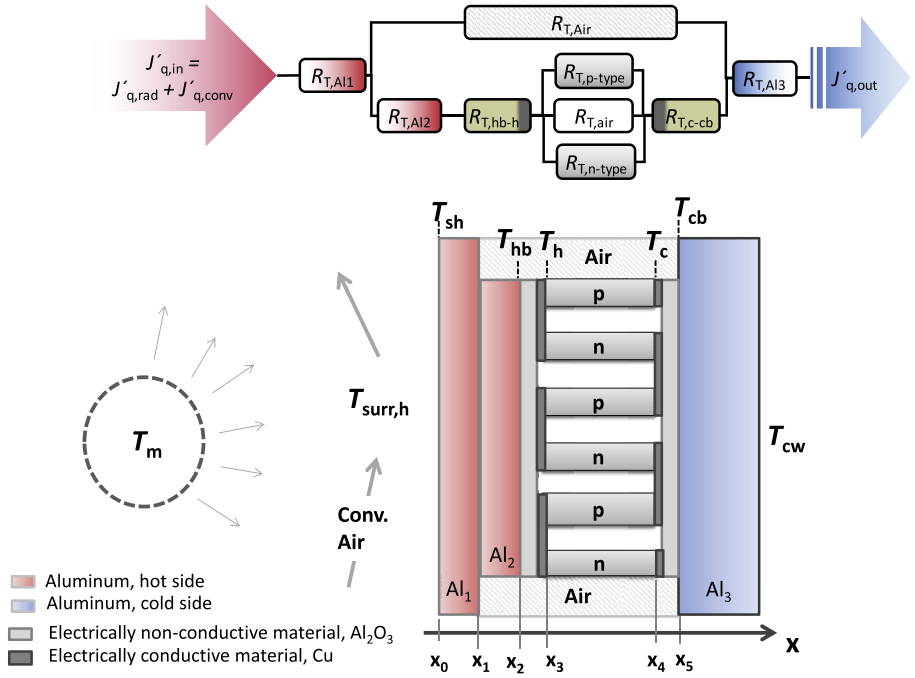

Fig. 3. The bottom figure shows a cross section of one building block of the thermoelectric generator model, and shows the different layers of Al, Al_2O_3, Cu, air and the p/n semiconductors. The top figure shows a thermal-electric network diagram where the different layers are represented as thermal resistances, R_T, that are connected in series and parallel. Apart from the R_T for the p and n type conductors, all thermal resistances are of the Fourier type. In the semiconductors, the heat flux is coupled to the charge flux.

sources and the melting temperature is high and remains high for long and starts to drop significantly with time only after all the silicon is solidified. Fig. 2b shows the casting area and the thermoelectric generator installed in the casting area. Next to the casting carousel, a 40 m^2 large wall is put up to shield sections of the plant from radiant heat given off from the silicon during casting. A window was cut in the wall and the thermoelectric generator was placed in this window, see Fig. 2b. During casting, high quality thermal energy was transferred from liquid silicon at temperature T_m, see Fig. 3, to the front side of the thermoelectric generator, mainly by radiant heat transfer. The radiant heat flux into the generator depended on the amount of silicon cast and the temperature of the silicon and varied throughout and between the casting periods. We estimated the air temperature inside the plant, $T_{surr,h}$ in Fig. 3, to 15 °C.

2.3. Testing procedure

The thermoelectric generator was installed in the casting area for a period of 40 h. During this period, the cooling water was flowing continuously and the temperatures were measured every five second. We defined an average temperature difference between the heating block and the cooling block side of the thermoelectric modules as:

$$\Delta T_{av} = \frac{\sum_{i=1}^{5} T_{hb,i}}{5} - \frac{\sum_{j=1}^{4} T_{cb,j}}{4} = T_{hb,av} - T_{cb,av} \quad (1)$$

Here, $T_{hb,i}$ is the heating block temperature measured at locations i = 1–5 and $T_{cb,j}$ is the cooling block temperature measured at locations j = 1–4, see Fig. 2a.

The generator was connected to a varying external, electronic load (Thurlby Thandar Instruments LD300, R_{ex} in Fig. 1). The electronic load controlled the generator electric potential, see Eq. (12). A LabView 2009 program regulated the electronic load and logged the external resistance, the generator potential and the current. Because the radiant heat flux into the generator varied throughout a casting period, the average temperature difference, Eq. (1), and thus the electric potential, Eq. (12), were never stable (see Fig. 4a). Therefore, we manually read the voltage every thirty second from the start of each casting period. When the voltage was stable within ±0.5 V for two readings or more, we activated the electronic load. The resistance was changed in steps of 0.5 Ω from 39.5 to 0 Ω. Because of highly transient temperature conditions, the load was regulated to measure for one second at each step.

We used polarization curves to describe the thermoelectric generator performance. A polarization curve is the electric potential plotted as a function of the electric current (see Eq. (12) and Fig. 5a). The generator power output was calculated from the corresponding values of the external load and the current, see Eq. (2), and plotted as a function of the current.

3. The mathematical model of the thermoelectric generator

In this section, we establish a mathematical model that has a sufficient level of complexity to capture the main characteristics of the experimental results, but at the same time is flexible enough to explore a large range of possible configurations of the TEG module. The thermal energy source in the present case has a transient behavior. However, we establish a stationary (time-average) model representation of the thermoelectric generator to examine how changes in the design influences the performance. We assume one dimensional heat transfer, which implies that all surfaces normal to the heat transfer direction are isothermal, and we neglect electric contact resistances and take the material properties to be temperature independent.

One unit in the thermoelectric generator model recapture (1/36) part of the generator described above. Each unit in the model (see Fig. 3) consists of one thermoelectric module kept between aluminum plates (Al_2 and Al_3). The module is made of *N* pairs of p-

Please cite this article in press as: Børset MT, et al., Exploring the potential for waste heat recovery during metal casting with thermoelectric generators: On-site experiments and mathematical modeling, Energy (2016), http://dx.doi.org/10.1016/j.energy.2016.10.109

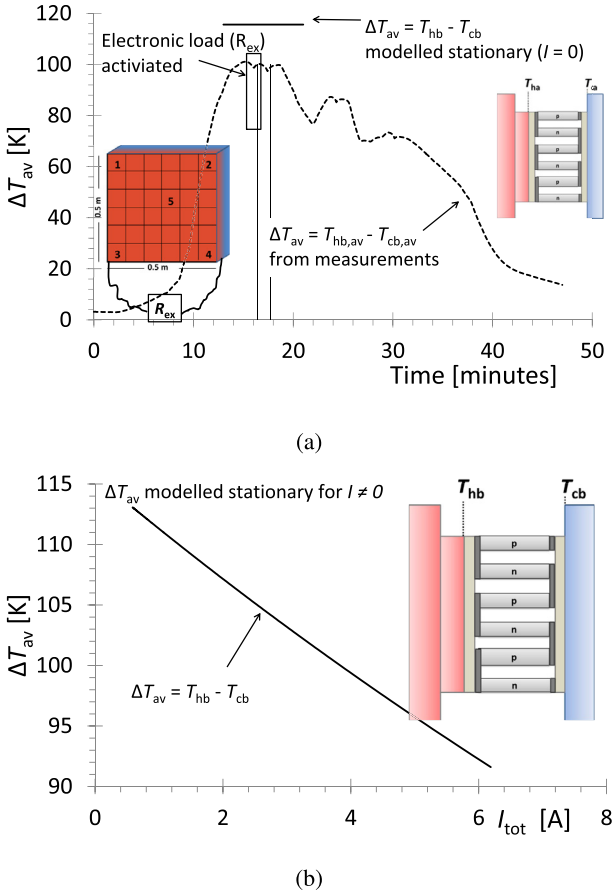

(a)

(b)

Fig. 4. a) The average temperature difference between the heating block and the cooling block for the thermoelectric generator, see Eq. (1), as a function of time for one casting period at the silicon plant. During this casting period, we activated the electronic load once as indicated in the figure. Also, the calculated temperature difference for the model of the thermoelectric generator when $I_{tot} = 0$ is included. b) The predicted temperature difference, between the heating block and the cooling block, as a function of the electric current for the model of the thermoelectric generator.

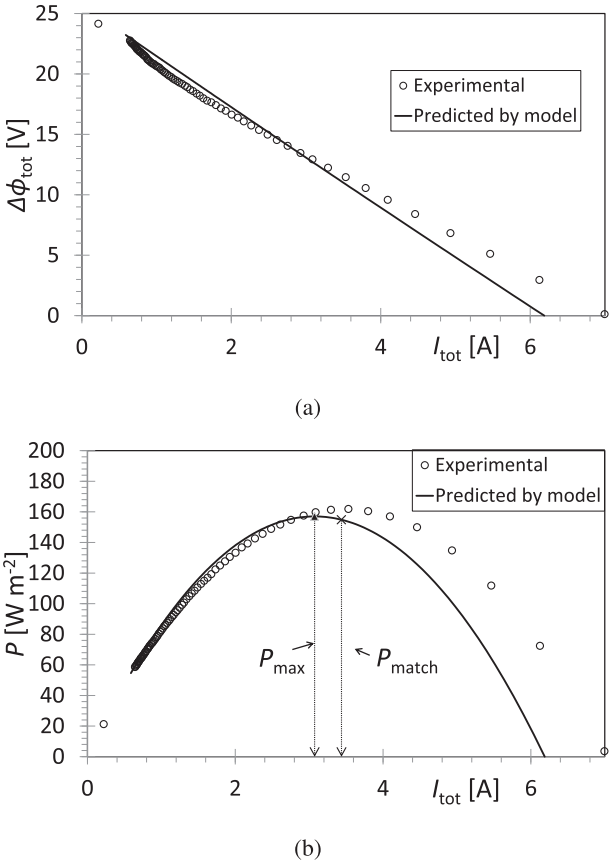

(a)

(b)

Fig. 5. a) The thermoelectric generator electric potential, $\Delta\phi_{tot}$, as a function of the electric current I_{tot}. The solid line is the polarization curve predicted by the stationary model. The circles represent the polarization curve obtained from the experiment run during the casting period in Fig. 4a. b) The electric power, P, produced by the thermoelectric generator per square meter of the generator (0.25 m^2) plotted as a function of the electric current I_{tot}. The solid line is the electric power predicted by the stationary model. The circles represent the electric power obtained from the experiment run during the casting period in Fig. 4a.

and n-types semiconductors ($N = 3$ in Fig. 3) connected electrically in series by copper strips and kept between two plates of aluminum oxide. The semiconductors are separated by an electrically non-conductive material which we take to be air (hereafter referred to using subscript **is**). There are two layers of aluminum at the left hand side of the module (Al_1 and Al_2) and one layer at the right hand side of the module (Al_3). The layers Al_1 and Al_2 make up the heating block in the experimental set-up while Al_3 is the cooling block (compare Figs. 2a and 3). The generator has N_s modules connected in series and N_p series are connected in parallel (*c.f.* Fig. 1).

We measured the power produced by the thermoelectric generator P as the power dissipated in a load with resistance R_{ex}. The steady-state energy balance of the whole generator is:

$$P = R_{ex} I_{tot}^2 = N_s N_p A\left(J'_{q,in} - J'_{q,out}\right) = \Delta\phi_{tot} I_{tot} \tag{2}$$

where $J'_{q,in}$ and $J'_{q,out}$ are the heat flux into and out of the generator at surfaces at positions x_0 and x_5 (see Fig. 3), A is the cross-sectional area of one unit, $\Delta\phi_{tot}$ is the generator terminal voltage and I_{tot} is the outer circuit current which relates to the current through each series of modules as $I_{tot} = N_p I_s$. We assume the heat fluxes to be uniform across the system's surface area.

3.1. Boundary conditions

High quality thermal energy ($N_p N_s A J'_{q,in}$) is transferred through radiation from the heat source (molten silicon) at temperature T_m to the surface at x_0 (see Fig. 3). By taking both radiative and convective heat transfer into account, the heat flux into the generator is (at x_0) [36]:

$$J'_{q,in} = c_{rad}\sigma\left(T_m^4 - T_{sh}^4\right) + h_{wh}\left(T_{surr,h} - T_{sh}\right) \tag{3}$$

where σ is the Stefan-Boltzmann constant. The parameter c_{rad} describes the radiative properties of the arrangement, including view factors [35,37], and h_{wh} is the convective heat transfer coefficient for the surface at x_0. The air surrounding this surface has the temperature $T_{surr,h}$. The heat flux out of the generator at x_5 is:

$$J'_{q,out} = U_{cb}\left(T_{cb} - T_{cw}\right) \tag{4}$$

where U_{cb} is the cooling block overall heat transfer coefficient.

3.2. Transport equations

The flux equations describing the transport of heat and charge through each semiconductor are [38]:

Please cite this article in press as: Børset MT, et al., Exploring the potential for waste heat recovery during metal casting with thermoelectric generators: On-site experiments and mathematical modeling, Energy (2016), http://dx.doi.org/10.1016/j.energy.2016.10.109

$$J'_{q,i} = -\lambda_i \frac{dT}{dx} + \frac{S_i^* T}{F} j_i \tag{5}$$

$$j_i = -\frac{S_i^*}{F r_i}\frac{dT}{dx} - \frac{1}{r_i}\frac{d\phi}{dx} \tag{6}$$

where subscript "i" refers to either the p- or the n-type semiconductor, λ_i is the thermal conductivity, F is Faraday's constant, r_i is the electrical resistivity and S_i^* is the transported entropy of the charge carrier. The transported entropies are functions of the material properties as well as the temperature and their sign can vary [39]. Equation (5) states that heat can be transported both by conduction and with the electric current. According to Eq. (6) we can use a temperature gradient to generate an electric potential gradient and an electric current. When there is no transport of charge, transport of thermal energy is by conduction only and Eq. (5) reduces to Fourier's law:

$$J'_q = -\lambda \frac{dT}{dx} \tag{7}$$

3.3. Temperature profiles

We use the energy balance to establish an expression for the temperature profiles for the semiconductors and the electrically non-conducting materials. We have the steady state energy balance for a volume element, assuming one-dimensional transport:

$$\frac{\partial}{\partial x}\left(J'_{q,i}\right) = \left(-\frac{\partial \phi(x)}{\partial x}\right) j_i \tag{8}$$

We find an expression for the gradient in electric potential from Eq. (6) and introduce this with Eq. (5) into the energy balance Eq. (8). The energy balance for each semiconductor becomes:

$$\frac{\partial}{\partial x}\left(-\lambda_i \frac{dT(x)}{dx} + \frac{S_i^* T(x)}{F} j_i\right) = r_i j_i^2 + \frac{S_i^*}{F} j_i \frac{dT(x)}{dx} \tag{9}$$

We assume constant material properties (λ_i, S_i^* and r_i) and use the boundary conditions $T(x_3) = T_h$ and $T(x_4) = T_c$ to solve Eq. (9) (see Fig. 3). At steady state conditions, we can then express the temperature profiles in the semiconductors as:

$$T_i(x) = -\frac{1}{2}\frac{r_i}{\lambda_i} j_i^2 x^2 + \left[\frac{(T_c - T_h)}{\delta_i} + \frac{1}{2}\frac{r_i}{\lambda_i} j_i^2 \delta_i\right] x + T_h \tag{10}$$

Here, δ_i is the thickness of semiconductor " i ". Similarly, we find a linear temperature profile for the electrically non-conducting materials:

$$T_{is}(x) = \frac{(T_c - T_h)}{\delta_{is}} x + T_h \tag{11}$$

In the modeling of the whole TEG, one can consider the layers of the TEG to be a set of thermal resistances, R_T connected in series and parallel. Following the thermal analogy of resistances in an electrical circuit, we can obtain the temperature at each interface between the layers, and the temperature profiles through each layer. A thermal-electrical network model diagram corresponding to a unit of the TEG is presented in the top part of Fig. 3. The figure elucidates that the heat flow that enters the outer surface of the TEG splits into parallel heat flows through the thermoelectric module and the surrounding layers of air. Also within the thermoelectric module, the heat flow splits into a parallel arrangement through the p/n semiconductors and the adjacent layers of air. Since the outer surface of the TEG (Al_1) consists of aluminum that has a very high thermal conductivity, we expect the thermal profile of the outer surface to be nearly uniform and the thermal spreading resistance to be negligible.

3.4. Thermoelectric power generation

From the energy balance for the thermoelectric converter, see Eq. (2), consisting of N_p modules in parallel and N_s modules in series, we find the expression for the electric power produced by the thermoelectric system:

$$P = R_{ex} I_{tot}^2 = \Delta\phi_{tot} I_{tot} = N_s \left[N\alpha_{pn}(T_h - T_c) - \left(r_n \frac{\delta_n}{A_n} + r_p \frac{\delta_p}{A_p}\right) I_s\right] I_{tot} \tag{12}$$

Here, the expression in the brackets at the right hand side equals the electric potential generated by one thermoelectric module, $\Delta\phi_m$. At zero current, the electric potential is proportional to the temperature difference across the semiconductors and it is lowered due to ohmic resistance when $I \neq 0$. As we shall see, since the current also carries heat due to coupling (see Eqs. (5)–(6)), it reduces the temperature difference. We neglect the ohmic resistance in the metal conductors, in the external leads and the contact resistances since their electrical resistances are low. The proportionality constant, α_{pn}, is the Seebeck coefficient of the semiconductor pair, defined as:

$$\alpha_{pn} = \frac{\left(S_p^* - S_n^*\right)}{F} = \left[\frac{\Delta\phi}{(T_H - T_C)}\right]_{I=0} \tag{13}$$

The electric potential is generated because there is a difference in the transported entropies of the charge carriers in the semiconductors. At reversible conditions ($I = 0$), the potential equals the difference between the heat absorbed reversibly at the hot side and the heat liberated reversibly at the cold side divided by Faraday's constant (neglecting the Thomson effect).

The magnitude of the current is set by the external resistance R_{ex}. From Eq. (12), with $I_{tot} = N_p I_s$, we express the current through each series as:

$$I_s = \frac{N_s N \alpha_{pn}(T_h - T_c)}{N_p R_{ex} + N_s N\left(r_p \frac{\delta_p}{A_p} + r_n \frac{\delta_n}{A_n}\right)} \tag{14}$$

We aim to maximize the power output (Eq. (2)) by varying the system design. Changing the design will affect the temperature profile in the system, and we need to solve the energy balance.

3.5. Model parameters

Tables 1 and 2 give model parameters that apply to the

Table 1
The cross-sectional areas A_i and thicknesses δ_i and for the parts that constitute one unit in the model of the thermoelectric generator (Fig. 3).

Property	Dimension	Value
$A = A_{Al_1} = A_{Al_3}$	m^2	$6.94 \cdot 10^{-3}$
$A_{Al_2} = A_{Al_2O_3} = A_m$	m^2	$1.60 \cdot 10^{-3}$
$A_p = A_n = A_{pn}$	m^2	$2.25 \cdot 10^{-6}$
δ_{Al_1}	m	$4.7 \cdot 10^{-3}$
δ_{Al_2}	m	$5.3 \cdot 10^{-3}$
$\delta_{Al_2O_3}$	m	$0.8 \cdot 10^{-3}$
δ_{Cu}	m	$0.5 \cdot 10^{-3}$
$\delta_p = \delta_n = \delta_{pn}$	m	$1.5 \cdot 10^{-3}$

Please cite this article in press as: Børset MT, et al., Exploring the potential for waste heat recovery during metal casting with thermoelectric generators: On-site experiments and mathematical modeling, Energy (2016), http://dx.doi.org/10.1016/j.energy.2016.10.109

experimental set-up (base case) and the casting situation. The cross-sectional areas (A_i) and thicknesses (δ_i) applied to all layers in the generator model (Fig. 3) are given in Table 1. All values are chosen to recapture the generator described in the Experimental section. With $N_s = N_p = 6$, the model of the thermoelectric generator consists of thirty six model units (one unit is pictured in Fig. 3). The model unit cross-sectional area A is (1/36) part of the cross-sectional area of the thermoelectric generator (0.25 m^2, see Fig. 2a). The cross-sectional area of one thermoelectric module in the model (A_m) is the same as for those used in the experimental set-up. The difference $A - A_m = A_{air}$. This gap is filled with air.

The ratio of the module cross-sectional area (A_m) and the total cross-sectional area (A) is the fractional area:

$$f_A = \frac{A_m}{A} \tag{15}$$

It relates to the fill-factor of the thermoelectric module:

$$f_{Am} = \frac{2NA_{pn}}{A_m} \tag{16}$$

Values for the heat transfer coefficients h_{wh}, c_{rad} and U_{cb} (see Eqs. (3) and (4)) as well as temperatures applicable to the thermoelectric generator and the casting situation, are given in Table 2 together with materials transport properties.

We estimated the convective heat transfer coefficient h_{wh} from the average Nusselt number, Nu, for natural convection from a vertical plate, at the surface temperature $T_{sh} = 200$ °C and with the characteristic length $L_c = 0.5$ m, to air at the surroundings temperature $T_{surr,h} = 15$ °C, see Figs. 2a and 3. We found the Nusselt number from the correlation $Nu = 0.59Ra^{1/4}$ [35] where Ra is the Rayleigh number. The surface temperature T_{sh} was equal to the maximum in the average heating block temperature, $T_{hb,av}$ (see Eq. (1)), from the measurements in the casting area at the silicon plant. Thus, the value given in Table 2 is an average of the maximum value reached during a casting period.

We estimated the parameter c_{rad} from the energy balance across the thermoelectric generator, Eq. (2), when no power was dissipated in the external load ($P = 0$). The heat absorbed by the generator was described by Eq. (3), where A was the generator cross-sectional area (0.25 m^2), while the heat leaving the generator was:

$$\left(AJ'_{q,out}\right) = UA\Delta T_{av} \tag{17}$$

Here $U = (102 \pm 3.2)$ W/(m^2 K) is the overall heat transfer coefficient of the thermoelectric generator. This was determined from steady state experiments, similar to the experiments reported in Ref. [16]. We used $T_m = 1400$ °C, $T_{surr,h} = 15$ °C and $T_{sh} = T_{hb,av}$. As inputs to the calculation of c_{rad}, we used ΔT_{av} and $T_{hb,av}$ from temperature measurements for $P = 0$. The temperature of the heat source, T_m, varied through a casting period while the value estimated for c_{rad} reflects the casting situation for a constant heat source temperature ($T_m = 1400$ °C). The parameter c_{rad} reached a maximum during each of the casting periods. The value given in Table 2 is the average peak value from seven casting periods. The uncertainty in c_{rad} represents the variation between the seven casting periods.

We estimated the heat transfer coefficient U_{cb} from Eqs. (4) and (17). We used $T_{cs} = T_{cb,av}$ and T_{cw} was the average of the cooling water inlet and outlet temperature. The large uncertainty in U_{cb} is due to the accuracy in the temperatures measured with the K-type thermocouples in the heating block and the cooling block.

We estimated the material properties α_{pn} and r_{pn} for steady state measurements, similar to the experiments reported in Ref. [16]. The Seebeck coefficient, from the slope of the open circuit potential plotted versus the average temperature difference (see Eq. (1)), was (300 ± 4) μV/K. The slope of the polarization curves gave an electrical resistivity equal to $1.95 \cdot 10^{-5}$ Ω m. This value includes the contact resistances and the electrical resistances in the electrical leads. The thermal conductivity was $\lambda_{pn} = 1.4$ W/(m K) [40].

Table 2
The thermal conductivities for the layers in the model in Fig. 3, the heat transfer properties and temperatures that applies to the base case representation of the casting situation.

Property	Dimension	Value
λ_{Al}	W m^{-1} K^{-1}	177 [35]
$\lambda_{Al_2O_3}$	W m^{-1} K^{-1}	36 [35]
λ_{Cu}	W m^{-1} K^{-1}	401 [35]
$\lambda_p = \lambda_n = \lambda_{pn}$	W m^{-1} K^{-1}	1.4 [40]
λ_{air}	W m^{-1} K^{-1}	0.034 [35]
$r_p = r_n = r_{pn}$	ohm m	$1.95 \cdot 10^{-5}$
α_{pn}	V K^{-1}	$300 \cdot 10^{-6}$
c_{rad}	–	0.0269 ± 0.0012
h_{wh}	W m^{-2} K^{-1}	6
U_{cb}	W m^{-2} K^{-1}	105 ± 47
T_m	°C	1400
$T_{surr,h}$	°C	15
T_{cw}	°C	6

4. Results and discussion

We first discuss the results obtained for the experimental set-up installed in the casting area in the silicon plant (*c.f.* Fig. 2b) which defines the base case. The experimental results are next compared to the predictions of the mathematical model. Finally, we use the model to evaluate the potential of TEG implementation and optimisation.

4.1. On-site measurements

The temperature difference across the semiconductors in the thermoelectric modules determines the potential for thermoelectric power generation (see Eqs. (2) and (12)). In the casting area, the radiant heat dominated the heat flux into the generator (see Eq. (3)) and determined the temperature difference across the modules (see Fig. 2a). Fig. 4a shows the variation in the average temperature difference ΔT_{av} (see Eq. (1) and Fig. 2a) throughout one casting period. The variation is due to fluctuations in the radiant heat reaching the surface of the generator, in turn caused by variation in the amount and temperature of the silicon in the course of the casting. Around 12 min into the casting, the average temperature difference reached a maximum of about 100 K and was stable at this value for some minutes before it decreased, stabilized at a lower value and then dropped off at the end of casting. The shape of this curve, shown in Fig. 4a, was typical for all casting periods.

Fig. 5a and b shows the generator polarization and power curve obtained by activating the electronic load (R_{ex} in Eq. (2)) at the time indicated in Fig. 4a. For a constant temperature drop across the semiconductors, we expect a linear polarization curve in accordance with Eq. (12). The polarization curve in Fig. 5a is, however, not perfectly linear. This may be caused by fluctuations in ΔT_{av} (Fig. 4a), as discussed above. Also, non-uniform temperatures in the heating and cooling block could contribute to this. The maximum power was 40.5 W or 162 W m^{-2}, taking the cross sectional area of the converter into account (0.25 m^2). Both the generator design and its location relative to the heat source can be utilized to enhance the performance of the generator as we shall discuss further below.

Please cite this article in press as: Børset MT, et al., Exploring the potential for waste heat recovery during metal casting with thermoelectric generators: On-site experiments and mathematical modeling, Energy (2016), http://dx.doi.org/10.1016/j.energy.2016.10.109

4.2. Comparing the model and the experimental results

We adapted the model to the TEG using the base case parameters described above. The model of the TEG gives a time-average description, where the boundary conditions we have used in the model correspond to the maximum in Fig. 4a. Fig. 6 shows the temperature profile at $I = 0$ through the generator. We observe that the largest temperature drop is across the semiconductor layer and that $T_{hb} \approx T_h$ and $T_{cb} \approx T_c$ (see also Fig. 3). In the model, we consider one-dimensional heat flow only and heat flow in parallel through the thermoelectric module feet and the adjacent and surrounding air. The central layer in the module (thermoelectric material) consists of semiconductors and air. The thermal conductivities are low (1% and 0.02% for semi conductor and air) compared to the neighbouring layers (aluminum), as can be read from Table 2. Thus we expect the temperature drop to be largest across the thermoelectric layer, which is also beneficial for power generation. A variation in the module size, or the cross-sectional areas of the semiconductors (*i.e.* the fractional areas, see Eqs. (15) and (16)), determines this temperature drop.

The model predicted ΔT_{av} to be 115 K at $I = 0$ which is 15% above the experimental maximum value of 100 K (*c.f.* Fig. 4a). The overall heat transfer coefficient (U, see Eq. (17)) of the TEG as predicted by the model was around 10% lower than the experimentally determined value (90 compared to 100 W m^{-2} K^{-1}). The magnitude of the heat loss to the environment by convection was approximately 10% relative to the heat incoming by radiation. A source of inaccuracy was that in the model, we neglected heat leakage via the screws running through the heating and cooling blocks and considered only one-dimensional heat transfer by conduction. For two screws of stainless steel, we estimate the heat flow through the screws from Fourier's law (Eq. (7))to account for about 8% of the heat flow through the generator with no screws (5 W compared to 60 W for $\Delta T = 100$ K). In this estimate, we assumed that the screws were made of stainless steel with thermal conductivity of 20 W m^{-1} K^{-1}, thickness of 10 mm and a diameter of 4 mm. This heat leakage thus explains the larger fraction of mismatch between the overall heat transfer coefficient predicted by the model and the experimentally determined value.

Fig. 4b shows the temperature difference across the modules as a function of current. This was found by solving the energy balance for a varying external load R_{ex}. The model predicted a 20% reduction in ΔT_{av} by going from zero current to 6.2 A, i.e. at $\Delta\phi_{tot} = 0$. This reduction is caused by the thermal energy moved reversibly with the current from the high to the low temperature side of the conductors i.e. the *Peltier heat*, *c.f.* Eq. (5). A reduction in ΔT_{av} was also observed experimentally when the electronic load was activated (see Fig. 4a), however, this reduction was smaller than predicted by the model. In the experiments, we recorded each current and voltage point for a second by regulating the external resistance R_{ex} and the conditions were non-stationary. This lead to some linear deviations in the graphical presentation of some of the data points.

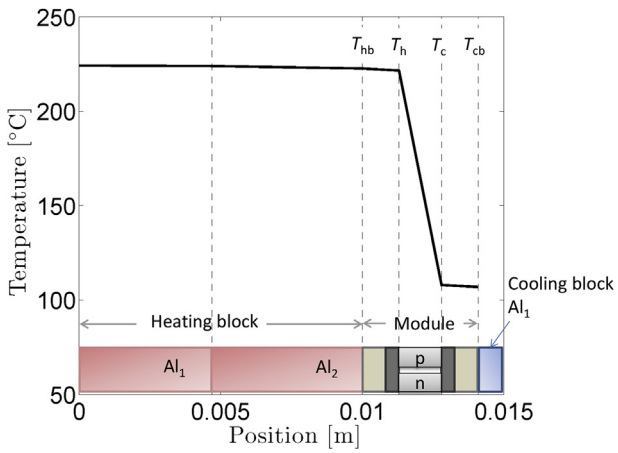

Fig. 6. The temperature as a function of position through the system as predicted by the model for $I = 0$. The different layers in the model are indicated, *c.f.* Fig. 3.

The polarization curve given by the model gave excellent predictions for the current as expressed by Eq. (12). As discussed above, the temperature difference decreased as the current increased. Thus both terms in Eq. (12) contribute to the slope of the polarization curve. Since we have used a stationary state model, the modest difference between the model and the experimental results mainly stem from transient behavior of the silicon casting process.

From the model, we predicted the maximum power to be 157 W m^{-2} (P_{max} in Fig. 5b) which is in good agreement with the experimentally determined value of 162 W m^{-2}. The power generated at the so-called matched load conditions (P_{match}), i.e. when the electrical resistance in the external load is equal in magnitude to the system's electrical resistance, is by definition taken as the maximum power. According to Fig. 5b, P_{max} is slightly larger than P_{match} and the corresponding current is slightly smaller for P_{max} than for P_{match}. However, the difference is small and we shall take $P_{max} = P_{match}$ in the following. A parameter which often is used to characterize technology for recovering waste heat is the thermal efficiency, defined as the ratio of the power to the heat inflow. In agreement with previous work on the topic, the thermal efficiency of the TEG was found to be between 1.5% and 4%, and was found to increase monotonically with the magnitude of c_{rad}. Since the most valuable component to the end-user is the power generated, we have not focused in detail on the thermal efficiency of the TEG in this work [15].

From the discussion above, we conclude that the steady-state model captures to a good accuracy the heat transfer characteristics and the experimentally determined polarization curve of the TEG. We shall therefore next use the model to study the potential for TEG implementation improvement.

4.3. Strategies for improving the performance of the TEG

We first discuss how we can increase the power generated by the system (P_{match}) by increasing the heat transfer coefficients c_{rad} and U_{cb} (see Eqs. (3) and (4)), but by keeping within temperature-limits of the thermoelectric modules. The c_{rad} describes the amount of heat delivered to the front panel of the TEG assembly while U_{cb} describes the heat sink capacity. In the present set-up, c_{rad} could have been changed by changing the location of the TEG assembly or having *e.g.* liquid iron instead of silicon and the heat sink capacity can be at least doubled by better integration between the copper tube and the aluminum on the TEG module cold side.

Next we discuss how we can further increase the power generated by the system by also reducing the fractional area f_A (see Eq. (15)). By exceeding the temperature limits of the materials the thermoelectric module will degrade and eventually stop functioning. The BiTe based thermoelectric modules applied in the current experimental set-up had upper limits of 380 and 160 °C for the hot and cold side respectively. We discuss the improvements within these limits.

In the experiments, the position of the thermoelectric generator relative to the heat source (molten silicon, see Fig. 2b) limited the thermal energy flux into the generator (Eq. (3)) and thus the power generated. By moving the generator closer to the heat source, and/or by changing its angle relative to the silicon surface, we can increase the heat flux into the generator ($J'_{q,in}$) and thus the power

Please cite this article in press as: Børset MT, et al., Exploring the potential for waste heat recovery during metal casting with thermoelectric generators: On-site experiments and mathematical modeling, Energy (2016), http://dx.doi.org/10.1016/j.energy.2016.10.109

generated (Fig. 7a). To increase the heat flux by a factor of 1.5, keeping all other parameters constant, increases the power generated by a factor of 2.2, from 160 to 350 W m^{-2}, without exceeding the operating temperature limits for the thermoelectric modules applied.

In the experimental set-up, the copper pipe-aluminum block contact area limited the heating block overall heat transfer coefficient U_{cb} (see *e.g.*, the Experimental section). For the heat flux, to double the contact area (*e.g.* doubling the length of the copper pipe or adding a thermal paste) is equivalent to doubling the U^0_{cb} value applicable to the experimental set-up (base case) which we believe is well within reach. Then we could increase the heat influx ($J'_{q,in}$) by a factor 2.5 and generate 900 W m^{-2}, without exceeding the temperature limits for the thermoelectric modules. We shall use $U_{cb} = 2h^0_{cb}$ below to investigate how we can further improve the power output by optimizing the cross-sectional area of the modules, expressed as the fractional area (f_A). Thus, the strategy for maximum power generation is to ensure as good heat transfer as possible with the cooling-pipes at the cold end of the TEG, and simultaneously ensure that the position of the TEG is sufficiently close to the heat source without compromising the temperature-limits of the materials.

We varied the parameter c_{rad}. For each value we numerically determined the fractional area (f_A, see Eq. (15)) that gave the largest power at matched load conditions (P_{match}). The fractional area was defined as the ratio of the total thermoelectric module area to the system's surface area.

Fig. 8 shows the matched load power (top), the fractional area (middle) and the temperature difference across the semiconductors $\Delta T_{av} = T_{hb} - T_{cb}$ (bottom) as a function of c_{rad}/c^0_{rad}. The solid lines represent the results that fulfill the operating temperature limits for both the hot and cold side of the thermoelectric module. The dashed lines are the results that violate the temperature limits.

The diagrams in Fig. 8 are to be read by drawing vertical lines from bottom to the top. First, we show this for the base case when $c_{rad}/c^0_{rad} = 1$ (indicated by the vertical red line). This left figure is constructed using the same U_{cb} as applies to the experimental set-up, hence our base case. This means that the diagram is tailored for any set-up of interest - as long as one knows the incoming heat (c_{rad}/c^0_{rad}) and the heat sink capacity (U_{cb}). Once these two first parameters are set, one can follow the red line upwards to the top graph. The intersection between the red line and the solid line gives the theoretical maximum power density, which in this instance is around 340 W m^{-2}. The next step is to search for what the lowest fractional area one can have is for the given radiation (c_{rad}/c^0_{rad}) and heat sink capacity (U_{cb}.) without violating the temperature limitations. This value is recognized in the middle graph at the intersection point between the red line and the solid line. We can now conclude that by lowering the fractional area, f_A, from the current value of 0.23 (blue horizontal dashed line) to around 0.06, one can have the power density of the TEG assembly increasing from around 160 to 340 W m^{-2}. The dashed black lines indicates the available potential for the system as a function of the incoming heat if no temperature boundaries are given. The solid black lines indicate the maximum power that one can have for the radiation heat when we account for the hot side and cold side temperature constraints. With the current heat sink capacity, U^0_{cb}, the systems cold side will be overheated if too much radiation heat is added. This is the reason why the solid lines ends in the base case figure in Fig. 8. To increase the radiation heat by more than a factor of 1.6, the heat sink capacity would have to increase.

In the "Improved case" in Fig. 8, we show the diagram when the heat sink capacity (U^0_{cb}) is doubled. That means that one can deliver twice as much heat without exceeding the temperature limit on the cold side. Doing so, one can also extract more work by reducing the fractional area further. Again, following the red line upwards, one can see that the matched load power is reached with a fractional area of 0.05 and that this power density is around 390. One can also see that the maximum heat one can have with the fractional area of the experimental setup is 2.5 times the one in our experiments.

In summary, by lowering the fractional area from 0.23 to 0.06 the power density increases from 160 to 340 W m^{-2}. By doubling the heat transfer in the cooling part the fractional area can be reduced further to 0.05 and the power density increased to 390 W m^{-2}. Thus, by tailoring the design of the TEG to the conditions encountered in the industrial facility, it is possible to generate more power with less thermoelectric material. The fractional area could even be reduced further, if the materials could sustain higher operating temperatures. When c_{rad} is increased beyond c^0_{rad}, we need to increase the fractional area to fulfill the temperature limits. At $c_{rad}/c^0_{rad} = 2.5$ the fractional area equals the fractional area for the experimental set-up. Beyond this limit, we need to increase the fractional area compared to the base case to fulfill the temperature limits.

The diagram in Fig. 8 shows the generator fractional area that maximize the matched load power output for a given location

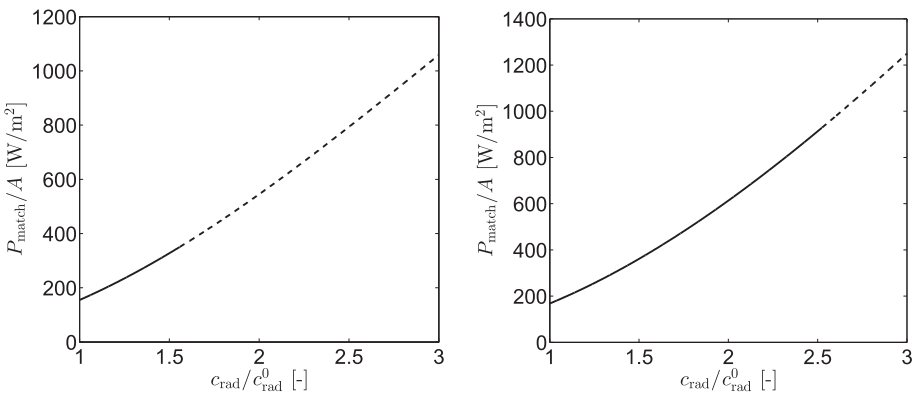

Fig. 7. The effect obtained by the generator at matched load conditions (P_{match}) as a function of the parameter c_{rad}. Here c^0_{rad} is the value that applies to the base case (experimental setting). The solid line represents the results for $T_{h,av} \leq T_{h,max}$ and $T_{c,av} \leq T_{c,max}$. The dotted line represents results where $T_{h,av} \geq T_{h,max}$ and $T_{c,av} \geq T_{c,max}$ where $T_{h,max} = 380$ °C and $T_{c,max} = 160$ °C is the maximum hot side and cold side operating temperature of the BiTe-based thermoelectric modules. In Fig. a) the cooling block overall heat transfer coefficient was $U_{cb} = U^0_{cb} = 105$ W $m^{-2}K^{-1}$ and in b) we used $U_{cb} = 2U^0_{cb}$.

Please cite this article in press as: Børset MT, et al., Exploring the potential for waste heat recovery during metal casting with thermoelectric generators: On-site experiments and mathematical modeling, Energy (2016), http://dx.doi.org/10.1016/j.energy.2016.10.109

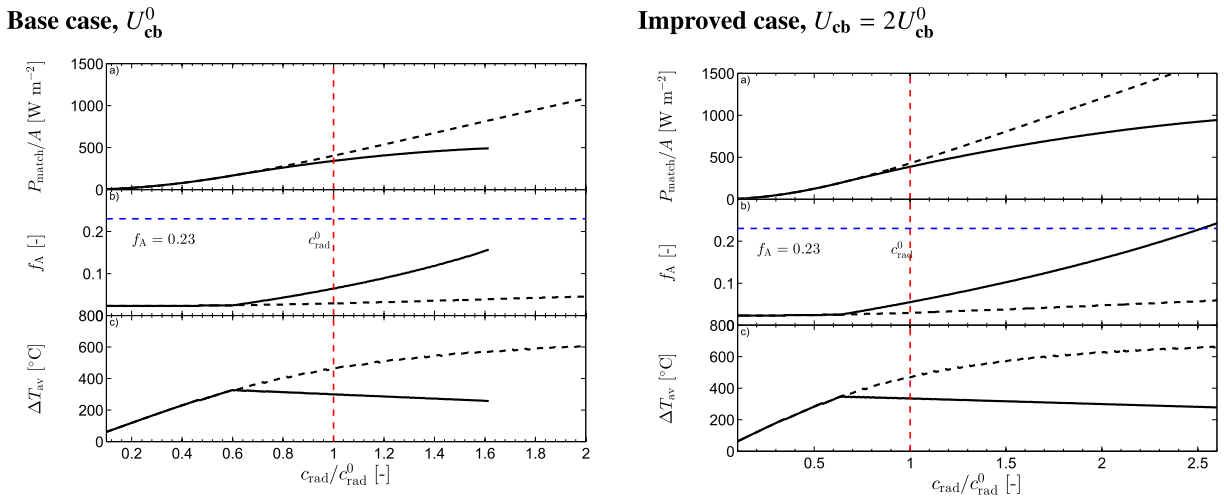

Fig. 8. The matched load power (top), the system fill factor f_A (middle) and the average temperature difference across the semiconductors (bottom) all plotted as a function of c_{rad} relative to c^0_{rad} (experimental conditions). The solid line represents the results for $T_h \leq T_{h,max}$ and $T_c \leq T_{c,max}$. The dotted line represents results where $T_h > T_{h,max}$ and/or $T_c > T_{c,max}$ where $T_{h,max} = 380$ °C and $T_{c,max} = 160$ °C is the maximum hot side and cold side operating temperature of the BiTe-based thermoelectric modules.

relative to the heat source, *i.e.* for a given c_{rad} value. The diagram also shows that employing materials that can sustain higher temperatures is beneficial to further enhance the potential for power generation. Based on the materials we have used (bismuth-tellurium based modules), we estimate that it is possible to recover as much as 900 W m^{-2} by enhancing the design and location of the thermoelectric generator.

5. Conclusions

In this work, we combined on-site experiments and a steady-state mathematical model to investigate the potential of thermoelectric power generation from heat available during casting of silicon. We implemented a 0.25 m^2 thermoelectric power generator (TEG) based on BiTe-modules in the casting area of a silicon plant and performed on-site measurements. The measured peak power was 160 W m^{-2} and the maximum temperature difference across the modules was 100 K (in this instance). The model revealed a significant potential to enhance the TEG performance beyond the experimental values through design and location relative to the heat source.

The strategy for maximum power generation is to ensure as good heat transfer with the heat sink at the cold end of the TEG, and simultaneously ensure a sufficiently heat flux into the TEG without compromising the temperature-limits of the materials. Based on the materials we have used (bismuth-tellurium based modules), we estimate that it is possible to generate as much as 900 W m^{-2} by enhancing the design and location of the thermoelectric generator.

Additionally, by tailoring the design of the TEG to the conditions encountered in the industrial facility, it is possible to generate more power with less thermoelectric material which is beneficial both from an economical perspective as well as from a resource use perspective. In the experimental set-up, the ratio of the cross-sectional area of thermoelectric modules to the system's surface area, the fractional area, was 0.23. This study showed that by reducing the number of modules by 50% could more than double the power output from the generator (400 versus 160 W m^{-2}).

Thermoelectric generators are scalable and simple systems that provide an opportunity to generate power from waste heat that is sporadically available like in casting of silicon, where we estimate that the thermoelectric generators with the BiTe technology have the potential to generate up to 900 W m^{-2}.

Acknowledgements

M.T.B. acknowledges the Research Council of Norway (project no. 193161) and the Norwegian Ferroalloy Producers Research Association for funding through the project “Fugitive emissions of materials and energy”. We acknowledge Elkem Salten for allowing measurements in the casting area and for practical arrangements at the plant. ENERSENSE is acknowledged for financial support.

References

[1] Kousksou T, Bruel P, Jamil A, El Rhafiki T, Zeraouli Y. Energy storage: applications and challenges. Sol Energy Mat Sol C 2014;120:59–80.
[2] Harman TC, Honig JM. Thermoelectric and thermomagnetic effects and applications. New York: McGraw-Hill; 1967.
[3] Seebeck TJ. Magnetiche polarisation der metalle und erze durch temperatur-differentz. Abh Kn Akad Wiss 1822:265–373.
[4] Huesgen T, Woias P, Kockmann N. Design and fabrication of MEMS thermoelectric generators with high temperature efficiency. Sens Actuat A-Phys 2008;145–146(1–2):423–9.
[5] Fleurial J-P. Thermoelectric power generation materials: technology and application opportunities. JOM 2009;61(4):79–85.
[6] Zebarjadi M, Esfarjani K, Dresselhaus MS, Ren ZF, Chen G. Perspectives on thermoelectrics: from fundamentals to device applications. Energy Environ Sci 2012;5:5147–62.
[7] Bubnova O, Crispin X. Towards polymer-based organic thermoelectric generators. Energy Environ Sci 2012;5(11):9345–62.
[8] Gunawan A, Lin C-H, Buttry DA, Mujica V, Taylor RA, Prasher RS, et al. Liquid thermoelectrics: review of recent and limited new data of thermogalvanic cell experiments. Nanosc Micros Therm 2013;17(4):304–23.
[9] Tasaka M. Thermal membrane potentialacross charged membranes and thermoosmosis. Pure Appl Chem 1986;58:1637–46.
[10] Janssen M, Härtel A, Van Roij R. Boosting capacitive blue-energy and desalination devices with waste heat. Phys Rev Lett 2014;113(26):268501.
[11] Sales BB, Burheim OS, Porada S, Presser V, Buisman CJ, Hamelers HV. Extraction of energy from small thermal differences near room temperature using capacitive membrane technology. Environ Sci Tech Lett 2014;1:356–60.
[12] Børset MT, Kang X, Burheim OS, Haarberg GM, Xu Q, Kjelstrup S. Seebeck coefficients of cells with lithium carbonate and gas electrodes. Electrochim Acta 2015;182:699–706.
[13] Kang X, Børset MT, Burheim OS, Haarberg GM, Xu Q, Kjelstrup S. Seebeck coefficients of cells with molten carbonates relevant to the metallurgical industry. Electrochim Acta 2015;182:342–50.
[14] Yee SK, LeBlanc S, Goodson KE, Dames C. $ per W metrics for thermoelectric power generation: beyond ZT. Energy Environ Sci 2013;6(9):2561–71.
[15] LeBlanc S, Yee SK, Scullin ML, Dames C, Goodson KE. Material and manufacturing cost considerations for thermoelectrics. Renew Sust Energy Rev 2014;32:313–27.
[16] Takla M, Burheim O, Kolbeinsen L, Kjelstrup S. A solid state thermoelectric power generator prototype designed to recover radiant waste heat. In: Energy technology 2012: carbon dioxide management and other technologies. John Wiley & Sons, Inc; 2012. p. 101–8.

Please cite this article in press as: Børset MT, et al., Exploring the potential for waste heat recovery during metal casting with thermoelectric generators: On-site experiments and mathematical modeling, Energy (2016), http://dx.doi.org/10.1016/j.energy.2016.10.109

[17] Chen J, Lin B, Wang H, Lin G. Optimal design of a multi-couple thermoelectric generator. Semi Sci Tech 2000;15:184–8.
[18] Suzuki RO, Tanaka D. Mathematical simulation of thermoelectric power generation with the multi-panels. J Power Sources 2003;122:201–9.
[19] Lineykin S, Ben-Yaakov S. Modeling and analysis of thermoelectric modules. IEEE T. Ind App 2007;43:505–12.
[20] Yu J, Zhao H. A numerical model for thermoelectric generator with the parallel-plate heat exchanger. J Power Sources 2007;172:428–34.
[21] Chen M, Rosendahl L, Condra T. A three-dimensional numerical model of thermoelectric generators in fluid power systems. Int J Heat Mass Tran 2011;54:345–55.
[22] Wang Y, Dai C, Wang S. Theoretical analysis of a thermoelectric generator using exhaust gas of vehicles as heat source. Appl Energy 2013;112:1171–80.
[23] Sahin AZ, Yilbas BS. The thermoelement as thermoelectric power generator: effect of leg geometry on the efficiency and power generation. Energy Conv Manage 2013;65:26–32.
[24] Rezania A, Rosendahl L, Yin H. Parametric optimization of thermoelectric elements footprint for maximum power generation. J Power Sources 2014;255:151–6.
[25] Barma M, Riaz M, Saidur R, Long B. Estimation of thermoelectric power generation by recovering waste heat from biomass fired thermal oil heater. Energy Conv Manage 2015;98:303–13.
[26] Gou X, Xiao H, Yang S. Modeling, experimental study and optimization on low-temperature waste heat thermoelectric generator system. Appl Energ 2010;87(10):3131–6.
[27] Meng F, Chen L, Sun F, Yang B. Thermoelectric power generation driven by blast furnace slag flushing water. Energy 2014;66:965–72.
[28] Niu X, Yu J, Wang S. Experimental study on low-temperature waste heat thermoelectric generator. J Power Sources 2009;188:621–6.
[29] Gunawan A, Fette NW, Phelan PE. Thermogalvanic waste heat recovery system in automobiles. In: Proceedings of the ASME 2015 power conference San Diego; 2015. POWER2015–49094.
[30] Chen W-H, Liao C-Y, Hung C-I, Huang W-L. Experimental study on thermoelectric modules for power generation at various operating conditions. Energy 2012;45:874–81.
[31] Liu C, Chen P, Li K. A 500 W low-temperature thermoelectric generator: design and experimental study. Int J Hydrogen Energy 2014;39(28):15497–505.
[32] Liu C, Pan X, Zheng X, Yan Y, Li W. An experimental study of a novel prototype for two-stage thermoelectric generator from vehicle exhaust. J Energy Inst 2016;89(2):271–81.
[33] Takla M, Kamfjord NE, Tveit H, Kjelstrup S. Energy and exergy analysis of the silicon production process. Energy 2013;58:138–46.
[34] Takla M, Kamfjord NE, Halvard T, Kjelstrup S. Exergy based efficiency indicators for the silicon furnace. Energy 2015;90:1916–21.
[35] Çengel YA. Heat and mass transfer: a practical approach. third ed. New York: McGrawHill; 2006.
[36] Wilhelmsen Ø, Johannessen E, Kjelstrup S. Energy efficient reactor design simplified by second law analysis. Int J Hydrogen Energy 2010;35(24):13219–31.
[37] Barry M, Ying J, Durka MJ, Clifford CE, Reddy B, Chyu MK. Numerical solution of radiation view factors within a thermoelectric device. Energy 2016;102:427–35.
[38] Kjelstrup S, Bedeaux D. Non-equilibrium thermodynamics of heterogeneous systems. Singapore: World Scientific; 2008.
[39] Jaime M, Hardner H, Salamon M, Rubinstein M, Dorsey P, Emin D. Hall-effect sign anomaly and small-polaron conduction in $(La_{1-x}\ Gdx)_{0.67}\ Ca_{0.33}\ MnO_3$. Phys Rev Lett 1997;78:951.
[40] accessed August Thermonamic Electronics, $Bi_2\ Te_3$-Based Thermoelectric Ingot (TIG-BiTe-P/N-1) for the thermoelectric cooling and power generation modules. 2013. URL, http://thermonamic.com/.

Please cite this article in press as: Børset MT, et al., Exploring the potential for waste heat recovery during metal casting with thermoelectric generators: On-site experiments and mathematical modeling, Energy (2016), http://dx.doi.org/10.1016/j.energy.2016.10.109